Nonlinear Dyn (2018) 93:653–669
https://doi.org/10.1007/s11071-018-4216-z

ORIGINAL PAPER

Dynamical analysis and multistability in autonomous hyperchaotic oscillator with experimental verification

T. Fozin Fonzin · J. Kengne · F. B. Pelap

Received: 15 June 2017 / Accepted: 10 March 2018 / Published online: 28 March 2018

Abstract In this contribution, a modified oscillator of Tamasevicius et al. (Electron Lett 33:542–544, 1997) (referred to as the mTCMNL oscillator hereafter) is introduced with antiparallel diodes as nonlinear elements. The model is described by a continuous time of four-dimensional autonomous system with hyperbolic sine nonlinearity based on Shockley diode model. Various methods for characterizing chaos/hyperchaos including bifurcation diagrams, Lyapunov exponents spectrum, frequency spectra, phase portraits, Poincaré sections and two parameter Lyapunov exponents diagrams are exploited to point out the rich dynamical behaviors in the model. Numerical results indicate that the system displays extremely rich dynamical behaviors including periodic windows, torus, chaotic and hyperchaotic oscillations. One of the main findings of this work is the presence of a region in the parameter space in which the mTCMNL experiences hysteretic behaviors. This later singularity/phenomenon is marked by the coexistence of multiple attractors (i.e., coexistence of asymmetric pair of periodic, torus and chaotic attractors with symmetric periodic, torus and chaotic attractors), for the same parameters settings. Basins of attractions of various competing attractors depicts symmetric complex basin boundaries, thus suggesting possible jumps between coexisting solutions (i.e., asymmetric pair of attractors with symmetric one) in experiments. A predominant route to chaos/hyperchaos observed in the system for different system parameters is the Afraimovich–Shilnikov scenario with tiny periodic regions. Experimental results from real-time circuit implementation are in good agreement with numerical analysis.

Keywords Multiple coexisting attractors · Hyperchaos · Two parameter Lyapunov exponent · Antiparallel diode · Experimental setup

T. Fozin Fonzin
Unité de recherche de Matière Condensée d'Electronique et de Traitement de Signal (LAMACETS), Faculty of Sciences, University of Dschang, P. O. Box 67, Dschang, Cameroon

T. Fozin Fonzin
Centre for Nonlinear Dynamics (CNLD), School of Physics, Bharathidasan University, Tiruchirappalli 620 024, India

T. Fozin Fonzin
Centre d'Excellence Africain en Technologies de l'Information et de la Communication (CETIC), University of Yaoundé I, P. O. Box 812, Yaoundé, Cameroon

J. Kengne
Unité de recherche d'Automatique et d'informatique Appliquée (LAIA), IUT-FV de Bandjoun, University of Dschang, P. O. Box 134, Bandjoun, Cameroon

F. B. Pelap (✉)
Unité de recherche de Mécanique et de Modélisation des Systèmes Physiques (L2MSP), Faculty of Sciences, University of Dschang, P. O. Box 69, Dschang, Cameroon
e-mail: fbpelap@yahoo.fr; francois.pelap@univ-dschang.org

1 Introduction

Shortly after Pecora and Carroll showed the possibility of synchronizing chaotic elements [2], many research

works have focused on applications and control of chaotic elements in different fields [3,4], as this phenomenon appears in many systems in a variety of ways. Secure communication [5–8] turns out as one of the prominent applications of chaotic signals. In 1995, after Perez and Cerdeira [9] have shown in their seminal work that masking signals with simple chaos (i.e., with only one positive Lyapunov exponent) does not provide high level of security, the design and implementation of suitable hyperchaotic generators [1,10–15] with more than one positive Lyapunov exponent have become one of the most followed research avenues. Among the various hyperchaotic generators, the circuit proposed by Tamasevicius et al. [1] (referred as TCMNL) comprising four memory elements, a p–n junction diode as the nonlinear component and a negative impedance converter attracted attention of recent times. Indeed, they adopted a piecewise linear model (PWL) of the diode to describe the dynamical behavior of the system. As PWL is merely a first-order approximation of the actual experimental circuit, Fozin et al. [16] proposed a smooth (exponential) mathematical model to investigate the nonlinear dynamics of the TCMNL oscillator. Moreover, they have also synchronized these coupled oscillators (considering smooth mathematical model) using nonlinear state observers. In 2015, Kengne [17] showed the coexistence of chaos with hyperchaos and also pointed out the striking phenomenon of transient chaos in the TCMNL oscillator by considering the smooth mathematical model of the diode as provided by the Schockley equation.

Very recently, many works [18–22] and references therein showed that by replacing the single diode (exponential function/nonlinear element) in many different circuits with antiparallel diode (hyperbolic function/nonlinear element) as suggested in [23], the whole dynamics of the system is changed and novel phenomena are exhibited. Using the same approach, we propose in this paper a modified TCMNL (referred as mTCMNL hereafter) with antiparallel diodes to uncover several dynamical behaviors of special interest. Due to the presence of antiparallel diodes (sine hyperbolic nonlinearity), the mTCMNL is highly symmetric and thus has potential to experience multiple coexisting attractors. Above the rich dynamics (chaos/hyperchaos) investigated in this work, we also provide a systematic and methodological analysis of the nonlinear dynamical mTCMNL oscillator helping to point out coexistence of multiple attractors. Indeed, while varying the system parameters, we observe the coexistence of multiple attractors (i.e., coexistence of three disconnected periodic attractors) ranging from periodic, torus to chaotic. More importantly, we provide the range of parameters set for which different dynamical behaviors exist and coexist.

Coexistence of multiple attractors is an interesting and striking phenomenon harnessed in the literature nowadays. Indeed, it has received lots of attention during the last decade in diverse areas such as electronic circuits [17,19,24–30], biological/ecological systems [31–33], laser [34], chemical reaction [35], just to name few. In contrast to monostable systems in which given set system parameters define a unique attractor, a multistable system may experience two (bistable) or more coexisting attractors for the same values of its parameters, depending solely on the choice of initial states [25–27,36]. Correspondingly, the state space is magnetized, and each coexisting attractor has its own sphere of influence called basin of attraction, (i.e., the set of initial conditions leading to long-time behavior that approaches the given attractor). Each attractor in the basin can display completely different properties such as Lyapunov exponents, frequency spectrum, and can appear in all combinations including fixed points, limit cycles, tori, chaotic attractors and hyperchaotic attractors (i.e., attractor with at least two positive Lyapunov exponents). The types and number of attractors may differ significantly depending on parameters monitoring/tuning. Consequently, the qualitative dynamic of the long-time behavior of a given nonlinear dynamical system can fundamentally change depending on which basin of attraction the initial state belongs. Though literature provides multiple coexisting attractors in asymmetric nonlinear systems [29,37], such phenomenon is mostly relevant/present in symmetric systems and may induce special events such as symmetry-breaking, symmetry restoring crisis, coexisting bifurcation and hysteresis [24,26,36]. The result presented here is then a rich contribution concerning symmetric autonomous hyperchaotic systems with simple/elegant mathematical model as well as electronic circuit realization [38]. One should notice that the coexistence of attractors is additional sources of randomness in chaotic systems and may be exploited for chaos-based secure communications or image processing [39]. However, their studies and control are very important in most engineering applications as they can lead to unexpected and potentially disastrous responses to perturbations

[35,40]. Detailed study along this line is beyond the scope of this work.

The paper is organized as follows. In Sect. 2, we briefly describe the mTCMNL circuit and a suitable mathematical model is derived to describe the dynamics of the proposed oscillator. Some basic properties of the model are underlined. The possibility of chaotic oscillations is presented from the stability analysis. Section 3 presents the result of our numerical investigation. The bifurcation structure showing the window of occurrence of coexisting multiple attractors is revealed. Phase portraits and corresponding Poincaré section/frequency spectra are depicted to confirm the bifurcation structure. The two parameter Lyapunov exponents corresponding to the two largest Lyapunov exponents are provided as abacus for engineering applications as they describe the whole dynamics in the system when varying simultaneously two control parameters. In Sect. 4, details studies of multistability in mTCMNL oscillator are depicted. Basins of attraction of various coexisting solutions are computed showing complex basin boundaries. Experimental results are presented in Sect. 5. Laboratory experimental measurements show a very good agreement with the theoretical analyses. Conclusion and possible future works are presented in Sect. 6.

2 Circuit description, mathematical model and basic properties

We briefly describe the circuit diagram in Sect. 2.1; then, in Sect. 2.2, we provide the corresponding mathematical model of the circuit diagram of mTCMNL. Finally, Section 2.3 presents the basic properties of the model and the nature of the equilibrium points.

2.1 Circuit description

The schematic diagram of the mTCMNL oscillator is depicted in Fig. 1. It consists of a combined parallel-series LC (namely $L_1C_1 - L_2C_2$), a negative impedance converter (NIC) $Z_{\mathrm{NIC}} = -R$ which is implemented as reported in [23] and two antiparallel diodes. The antiparallel diodes are responsible for the whole set of nonlinear phenomena (chaos/ hyperchaos) in the circuit and replace the only diode which was considered in the original circuit. During our analysis, $Z_{\mathrm{NIC}} = -R$ will serve as the main bifurcation control parameter for the system.

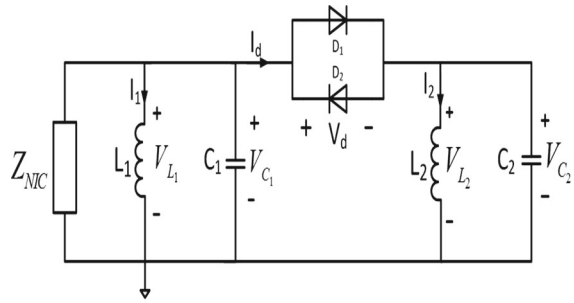

Fig. 1 Schematic diagram of the modified TCMNL oscillator with antiparallel diodes. Z_{NIC} is a negative impedance converter and is implemented as in [23]

2.2 Mathematical model

This subsection introduces the mathematical model of the mTCMNL considering the following hypothesis. Firstly, we assume all the components except the antiparallel diodes to operate in their linear region. Secondly, the current–voltage $(I - V)$ characteristic of each diode is modeled with an exponential function [16]. Hence, the overall current I_{d} flowing through the antiparallel diodes is described with a hyperbolic nonlinearity [18,19].

$$I_{\mathrm{d}} = f(V_{\mathrm{d}}) = 2I_s \sinh\left(\frac{V_{\mathrm{d}}}{\eta V_T}\right), \tag{1}$$

where I_s is the saturation current of the junction, V_{d} represents the voltage drop across the diode, η stands for the ideality factor $(1 < \eta < 2)$ and $V_T = k_B T/q$ is the thermal voltage. Here, K_{B} is the Boltzmann constant, T is the absolute temperature expressed in Kelvin and q is the electron charge. It is worth to note that at room temperature (300 K), we have $V_T \approx 26\,\mathrm{mV}$. By applying the Kirchhoff's laws to Fig. 1, we obtain the following set of autonomous differential equations of the mTCMNL oscillator:

$$\begin{cases} C_1 \dfrac{\mathrm{d}V_{C_1}}{\mathrm{d}t} = \dfrac{V_{C_1}}{R} - I_1 - I_{\mathrm{d}} \\ L_1 \dfrac{\mathrm{d}I_1}{\mathrm{d}t} = V_{C_1} \\ C_2 \dfrac{\mathrm{d}V_{C_2}}{\mathrm{d}t} = I_{\mathrm{d}} - I_2 \\ L_2 \dfrac{\mathrm{d}I_2}{\mathrm{d}t} = V_{C_2} \end{cases} \tag{2}$$

where I_n $(n = 1, 2)$ is the current flowing through the inductor L_n, V_{C_m} $(m = 1, 2)$ the voltage across capacitor C_m and I_d, defined by Eq. (1), is the current flowing through antiparallel diodes. We normalize the above set of first-order differential equations (2) by considering the following rescaled variables and parameters: $\tau = t/\sqrt{L_1 C_1}$, $V_\mathrm{ref} = \eta V_T$, $x_1 = V_{C_1}/V_\mathrm{ref}$, $x_2 = \rho I_1/V_\mathrm{ref}$, $x_3 = V_{C_2}/V_\mathrm{ref}$, $x_4 = \rho I_2/V_\mathrm{ref}$, $\alpha = \rho/R$, $\gamma = \rho I_s/V_\mathrm{ref}$, $\varepsilon_1 = C_1/C_2$, $\varepsilon_2 = L_1/L_2$ and $\rho = \sqrt{L_1/C_1}$. Consequently, we obtain the following system of smooth normalized differential equations:

$$\begin{cases} \dot{x_1} = \alpha x_1 - x_2 - f(x_1 - x_3) \\ \dot{x_2} = x_1 \\ \dot{x_3} = \varepsilon_1 \left(f(x_1 - x_3) - x_4\right) \\ \dot{x_4} = \varepsilon_2 x_3 \end{cases} \tag{3}$$

where $\dot{()} = \frac{\mathrm{d}}{\mathrm{d}\tau}$ and $f(x_1 - x_3) = 2\gamma \sinh(x_1 - x_3)$ is the hyperbolic nonlinearity of the system. Note that the presence of this hyperbolic nonlinearity is responsible of all the complex behaviors observed in system (3). The vector field associated with Eq. (3) is of C^∞ type due to the smoothness of the nonlinear hyperbolic function, thereby, making the system more tractable.

2.3 Symmetry and fixed points

From Eq. (3), one can easily check that the model is symmetric about the origin $O(0, 0, 0, 0)$, i.e., if $(x_1(\tau), x_2(\tau), x_3(\tau), x_4(\tau))$ is the solution of the system (3) for a specific set of parameters, then $(-x_1(\tau), -x_2(\tau), -x_3(\tau), -x_4(\tau))$ is also a solution for the same parameters set. As a consequence, any projection of the attractors in the (x_1, x_2, x_3, x_4) subspace or any lower combination is symmetric with respect to the origin; otherwise, they must appear in pairs, to restore the exact symmetry of the model equations. This exact symmetry could serve to justify the occurrence of several coexisting attractors in state space. Furthermore, this interesting property represents a good way to test the scheme used during numerical computation. The equilibrium point of system (3) is computed to be the origin $O(0, 0, 0, 0)$. The evaluation of the eigenvalues for the following chosen parameters set, $\alpha = 1.3$, $\varepsilon_1 = 3.228$, $\varepsilon_2 = 15.0$, $\gamma = 4.8982907 \times 10^{-5}$ yields: $\zeta_{1,2} = 0.649951 \pm j0.759976$ and $\zeta_{3,4} = -7.34746 \times 10^{-4} \pm j6.95845$. Consequently, as the eigenvalues are complex conjugate with some positive real parts, the equilibrium point $O(0, 0, 0, 0)$ is an unstable saddle focus. Physically, this result supports the fact that the oscillator can oscillate chaotically and excludes the existence of stable fixed point motion in the system (3).

3 Numerical analysis

The transitions to chaos/hyperchaos are defined by solving Eq. (3) numerically using the fourth-order Runge–Kutta method. For each set of parameter used in this work, the time step is always chosen as $\Delta t = 1 \times 10^{-4}$ during the computation. The system is integrated for a sufficiently long time, and the transient is discarded. Bifurcation diagram and Lyapunov exponent spectrum are the two combined indicators used in Sect. 3.1 to identify the type of transitions which lead to chaos/hyperchaos. Section 3.2 deals with the two parameter Lyapunov exponents diagrams which is an abacus for engineers to choose the right parameters sets for any further applications.

3.1 Bifurcation analysis

Bifurcation diagram is a qualitative tool to examine the transitions occurring in a dynamical system [41]. The variation of the local maxima of the state variable $x_2(\tau)$ with respect to the control parameter α is plotted in Fig. 2a, b. The final state at each iteration of the bifurcation control parameter is used as the initial condition for the next iteration. Two sets of data corresponding, respectively, to increasing (red) and decreasing (blue) values of α are presented. This strategy represents a straightforward method to identify the domains in which system (3) demonstrates the behavior of multiple coexisting attractors' (see Sect. 4 for more details). In the light of Fig. 2, one can easily observe that system (3) evolves from period-1 to chaos/hyperchaos oscillations/solutions with tiny windows of multiperiodic, quasiperiodic and chaotic attractors. These latter transitions are confirmed and characterized using the quantitative tool of Lyapunov exponent spectrum [42]. Table 1 quantifies the predominant phenomena of the mTCMNL in terms of Lyapunov exponents (LE) and also their corresponding ranges in terms of the control parameter α.

Using the same strategy as described to obtain the bifurcation diagrams, we have plotted in Fig. 2c, d, the

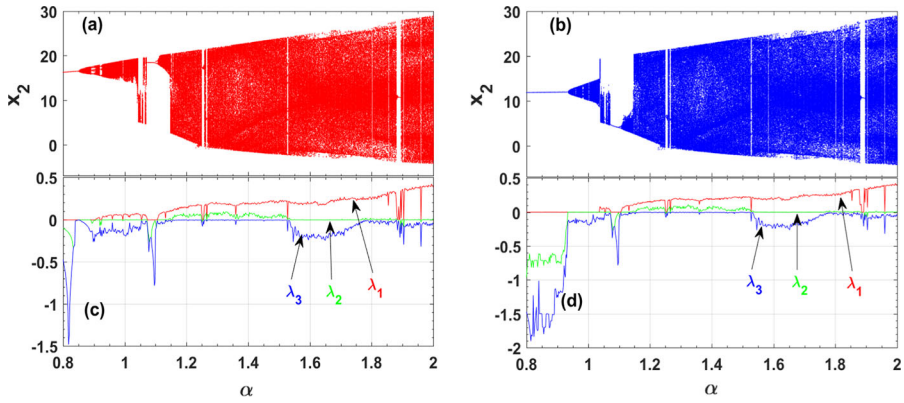

Fig. 2 Bifurcation diagrams **a**, **b** of two sets of data (corresponding to increasing (in red) and decreasing (in blue), respectively, the control parameter) showing the local maxima of the variable x_2 and their corresponding Lyapunov exponent spectrums **c**, **d** when the control parameter is varying within the range $0.8 \leq \alpha \leq 2.0$. A window of hysteresis can be notified when $\alpha \in [0.8; 1.037]$. The rest of the system parameters are $\varepsilon_1 = 3.228$, $\varepsilon_2 = 15$, $\gamma = 4.8982907 \times 10^{-5}$. (Color figure online)

Table 1 Characteristics of the various solutions of system (3) while increasing α

Solution	Lyapunov exponents	Range of the control parameter α
Periodic	$\lambda_1 = 0\,;\lambda_{2,3,4} < 0$	[0.8, 0.852]∪]1.069, 1.109]∪]1.884, 1.9]
Quasiperiodic (for 2D-torus)	$\lambda_{1,2} = 0\,;\lambda_{3,4} < 0$	]0.852, 0.8883]
Chaos	$\lambda_1 > 0\,;\lambda_{2,3,4} < 0$	]0.9284, 1.069]∪]1.522, 1.884]∪]1.9, 2.0]
Hyperchaos	$\lambda_{1,2} > 0\,;\lambda_{3,4} < 0$	]1.153, 1.249]∪]1.262, 1.522]

corresponding Lyapunov exponent spectrums for different values of $\alpha \in [0.8; 2.0]$. One can easily notice that the Lyapunov exponent spectrum of Fig. 2c (resp. Fig. 2d) well matches with the bifurcation diagram of Fig. 2a (resp. Fig. 2b). In opposition to the bifurcation diagram, the graph of Lyapunov exponent spectrum is a powerful tool to quantify chaos/ hyperchaos and also to distinguish chaos from quasiperiodic regions as it can clarify the bifurcation diagram which is only for qualitative characterization. More tools such as phase portraits and Poincaré section are also useful in this case. It can be seen that the bifurcation diagram well matches with the spectrum of the LE. Regions with single positive LE are simply chaotic, while those with two positive LE are hyperchaotic. Also, from Fig. 2c, d, parameter space for which the two largest LE equal to zero are called 2D-torus while those with the largest LE been equal to zero with all others negative are periodic regions (see Table 1). Using the same values of parameters in Fig. 2 combined with the symmetry property of the system, various phase portraits and corresponding Poincaré sections were computed to confirm different bifurcation sequences of Fig. 2a depicted previously (see Fig. 3). Asymmetric pair of attractors are depicted in Fig. 3a(1)–a(4), while double-band of strange hyperchaotic and chaotic attractors are observed in Fig. 3a(5), a(6), respectively. More information about the complexity of the attractors is provided through the double side 3D Poincaré sections [see Fig. 3b(1)–b(6)] across the hyperplane $x_4 = 0$. One can easily notice that the Poincaré section of hyperchaos oscillations is dense/disorder compared to those of chaotic oscillations. Also, torus is clearly represented with circle in the Poincaré section, while periodic motions are represented by sample of points which correspond to trajectories which are crossing the Poincaré hyperplane. The phase portraits corresponding to the coexisting region of the bifurcation diagram in Fig. 2a, b are well described/studied in Sect. 4.

3.2 Two parameter Lyapunov exponents

This section presents a two parameter Lyapunov exponents (LE) abacus for further application in engineering. As in the pioneering work of Tamasevicius et al. [1], inductances (i.e., ε_1) and capacitors (i.e., ε_2) were

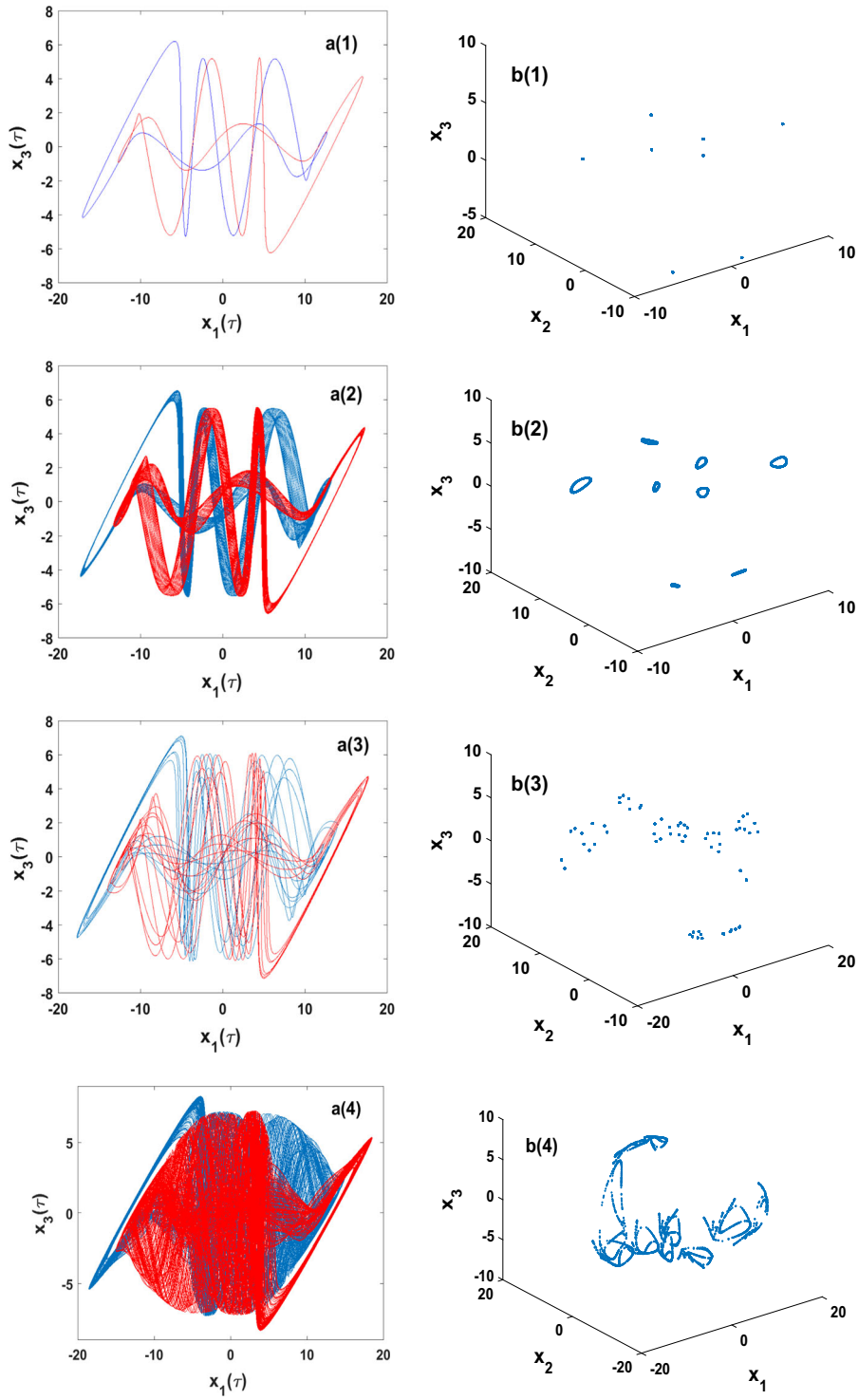

Fig. 3 Numerical phase portraits (left) of the mTCMNL oscillator and their corresponding 3D Poincaré section (right) in the hyperplane $x_4 = 0$ when varying α: **a(1)–b(1)** asymmetric period-1 for $\alpha = 0.85$; **a(2)–b(2)** asymmetric 2D torus for $\alpha = 0.86$; **a(3)–b(3)** asymmetric period-7 for $\alpha = 0.90$; **a(4)–b(4)** asymmetric single-band chaos for $\alpha = 0.95$; **a(5)–b(5)** symmetric double-band hyperchaos for $\alpha = 1.30$; **a(6)–b(6)** symmetric double-band chaos for $\alpha = 1.60$. Pair of asymmetric attractors are obtained using the following set of initial conditions (IC) chosen within the basin of attraction of IC : $(x_1(0), x_2(0), x_3(0), x_4(0)) = (\pm 0.5, \pm 1.0, \pm 0.5, \pm 0.3)$ while any combinations lead to symmetric double-band attractors

modeled with gyrators; hence, it is advantageous to consider either ε_1 or ε_2 (or both) as control parameters. The analysis of systems using two parameter LE through the construction of appropriate colorful diagrams by varying simultaneously two parameters of the system with the color as the intensity of the cho-

Fig. 3 continued

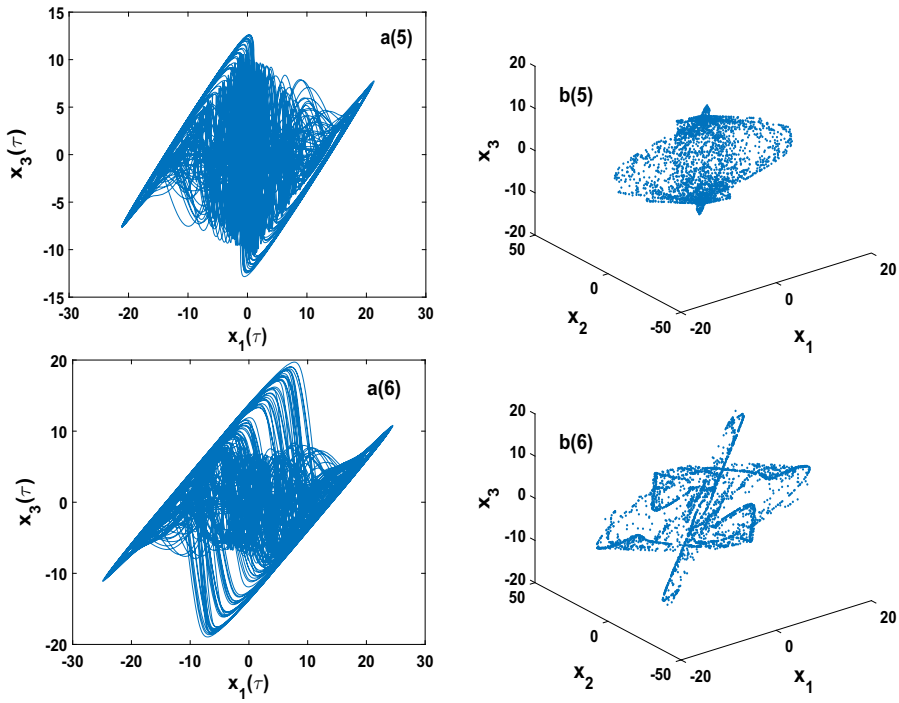

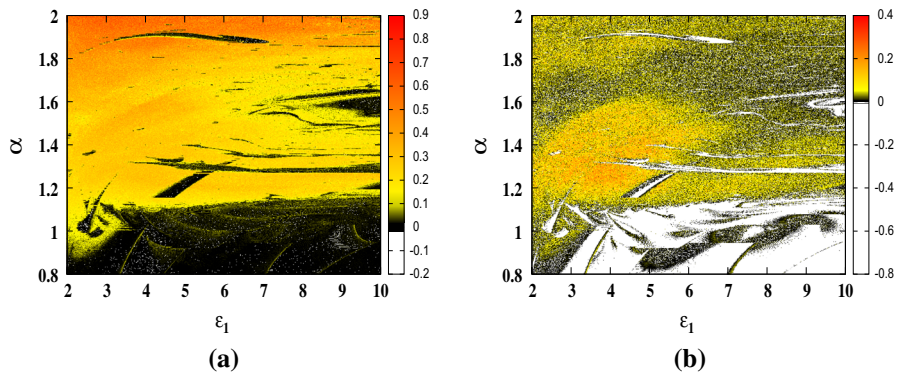

Fig. 4 Two parameter Lyapunov exponent diagram showing the largest (**a**) and the second largest (**b**) LE in the $(\alpha - \varepsilon_1)$ space helping to characterize hyperchaos, chaos, periodic solutions in system (3). The control parameters are varied within the ranges $0.8 \leq \alpha \leq 2.0$, $2 \leq \varepsilon_1 \leq 10$ and the rest of system parameters are fixed as: $\varepsilon_2 = 3.228$ and $\gamma = 4.8982907 \times 10^{-5}$

sen LE is not new. Indeed, literature [43,44] (and references therein) provides the analysis of largest LE as a tool to analyze and describe system with higher order. However, regarding four-dimensional systems, few works reported their complex behaviors using the LE spectrum to construct colorful two parameter LE diagram based on the largest and second largest exponents. Moreover, diagrams depicted here present the general dynamic of the system/oscillator when varying simultaneously two parameters. Henceforth, it is the main motivation of this section.

Firstly, Figure 4 presents the two parameter LE diagrams for the largest exponent (Fig. 4a) and for the second largest exponent (Fig. 4b), in the $(\alpha - \varepsilon_1)$ parameter space. Secondly, Figure 5 presents the two parameter LE diagrams for the largest exponent (Fig. 5a) and for the second largest exponent (Fig. 5b), in the $(\alpha - \varepsilon_2)$ parameter space. And finally, in Fig. 6 we have plotted the two parameter LE diagrams for the largest

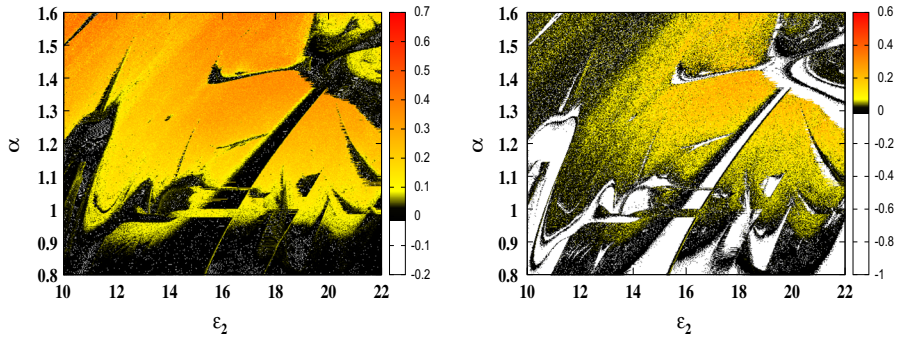

Fig. 5 Two parameter Lyapunov exponent diagram showing the largest (**a**) and the second largest (**b**) LE in the $(\alpha - \varepsilon_2)$ space helping to characterize hyperchaos, chaos, periodic solutions in system (3). The control parameters are varied within the ranges $0.8 \leq \alpha \leq 1.6$, $10 \leq \varepsilon_2 \leq 22$ and the rest of system parameters are fixed as: $\varepsilon_1 = 15$ and $\gamma = 4.8982907 \times 10^{-5}$

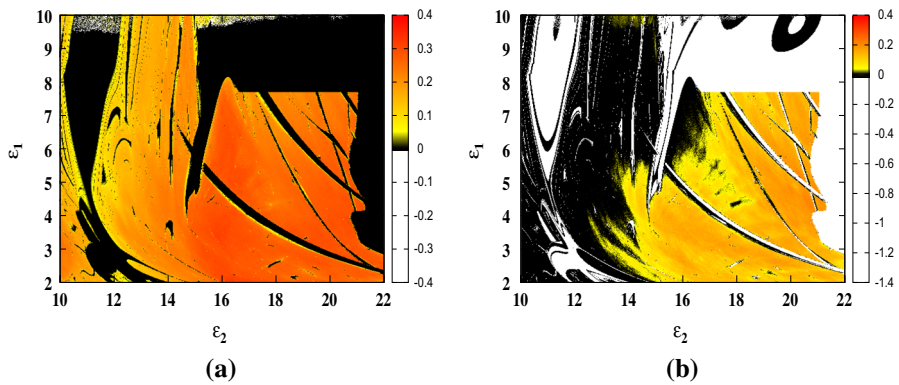

Fig. 6 Two parameter Lyapunov exponent diagram showing the largest (**a**) and the second largest LE (**b**) in the $(\varepsilon_2 - \varepsilon_1)$ space helping to characterize hyperchaos, chaos, periodic solutions in system (3). The control parameters are varied within the ranges $2 \leq \varepsilon_1 \leq 10$, $10 \leq \varepsilon_2 \leq 22$ and the rest of system parameters are fixed as: $\alpha = 1.3$ and $\gamma = 4.8982907 \times 10^{-5}$

exponent (Fig. 6a) and for the second largest exponent (Fig. 6b), in the $(\varepsilon_1 - \varepsilon_2)$ parameter space. In these figures (Figs. 4, 5, 6), the colorful diagrams are obtained by numerically computing LE spectrum on a grid of 500×500 values of the chosen space parameters. Moreover, the system (3) was integrated with a fourth-order Runge–Kutta algorithm with a fixed step size equal to 2×10^{-3}, considering 1×10^6 steps to compute the LE spectrum. Colors are associated with the magnitude of the LE as follows: White stands for the most negative, black for zero, red for the most positive, while positive exponent is indicated by a continuously changing yellow–red scale. In all these Lyapunov diagrams, we observe an abundant presence of periodic structures spread in chaotic and hyperchaotic regions. These periodic structures appear more clearly on the second largest exponent diagrams, as white structures embedded in black and yellow-reddish regions of Figs. 4b, 5 and 6b. Chaotic regions are characterized as a combination of yellow-reddish color on the largest LE diagram (Figs. 4a, 5, 6a) and a white and black color on the second largest LE diagram (Figs. 4b, 5, 6b), while hyperchaos is characterized by the combined yellow-reddish color on both the largest LE diagrams (Figs. 4a, 5, 6a) and second largest LE diagrams (Figs. 4b, 5, 6b). Some tiny windows of fixed points are also observed and are characterized with a white color on the largest LE diagram. One can notice a wider range of hyperchaos in the $(\varepsilon_1 - \varepsilon_2)$ parameter space of Fig. 6 than those of Figs. 4, 5. Indeed, a wider region of hyperchaos is observed in the second largest Lyapunov exponents for lower values of ε_1 and higher values of ε_2. Henceforth, the abacus of Fig. 6 is more appropriate in engineering applications such as secure communications due

to that broad band of hyperchaos. The two parameter LE are also useful to observe the different transitions which occur while scanning the two parameters space; hyperchaos to chaos and chaos to periodic behaviors are characterized, respectively, by yellow-reddish and yellow-blackish color transitions on the second largest LE diagram. This can be an alternative to recurrence plot [45,46] methods when analyzing these transitions for higher order (order ≥ 4) systems.

4 Coexistence of multiple attractors

With reference to the bifurcation diagram of Fig. 2 and the corresponding zoom depicted in Fig. 7, a wide window of hysteresis dynamics (and thus multiple stability) can be identified in the range $0.8 \leq \alpha \leq 1.037$. The three maximum Lyapunov exponents for increasing values of α are plotted in Fig. 7ii, while those corresponding to decreasing values are depicted in Fig. 7iii. A perfect correspondence can be noted between each set of bifurcation diagrams and its corresponding Lyapunov exponents diagram. From the bifurcation diagrams of Fig. 7i, two main routes (i.e., the formation and destruction of two-dimensional invariant tori) can be identified while varying the control parameter α. Route **I** (see Sect. 4.1) is the observed bifurcation scenario while decreasing the control parameter (bifurcation diagram of Fig. 7 in blue color), while route **II** (see Sect. 4.2) is the bifurcation scenario when the control parameter is increased (bifurcation diagram of Fig. 7 in red color). Table 2 provides a summary of the related coexisting attractors in each region of Fig. 7. The transition observed in route **I** is chaotic oscillations which breakdown to quasiperiodic oscillations and then limit cycle (see bifurcation diagram of Fig. 7i with red color). While in route **II**, the completely reverse previous transition is observed (bifurcation diagram of Fig. 7i in blue color) [47]. Despite the fact that route **I** and **II** depict each other reverse transitions, each route display completely different properties (phase portraits, frequency spectrum, Poincaré section just to name few). The attractor obtained in each route depends on the set of initial conditions leading to the long-time behavior that approaches the given attractor. Table 2 summarizes the overall attractors which are coexisting in each region of Fig. 7. Mainly, three attractors are coexisting; that is, one symmetric attractor obtained from route **I** and pair of asymmetric attractors obtained from route **II**. The corresponding phase portraits in each region of Fig. 7 are obtained by fixing the system parameters and then varying only the initial conditions (see Fig. 11).

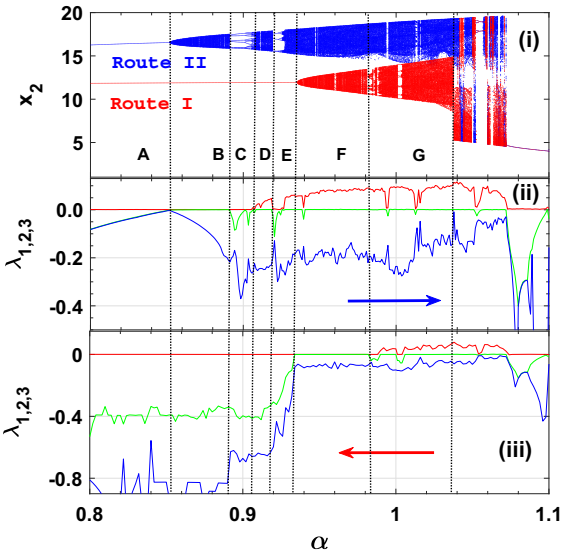

Fig. 7 Enlarged bifurcation diagrams (**i**) and its corresponding Lyapunov exponents (**ii, iii**) showing the phenomenon of hysteresis when decreasing (red color) and increasing (blue color) the control parameter α in the interval $[0.8 - 1.1]$. It is worth mentioning that attractors obtained from route I (red color bifurcation diagram) are symmetric with respect to the origin while asymmetric pair of attractors are obtained from route II (blue bifurcation diagram); see Table 2 for more (Color online)

4.1 Route I: transition from a stable cycle to chaos through a torus break down

When decreasing the control parameter α from 1.1 to 0.8, the following symmetric attractors are captured in the coexisting region of the control parameter ($0.8 \leq \alpha \leq 1.037$): chaos $\longrightarrow$ torus $\longrightarrow$ limit cycle with a tiny periodic windows as transition from chaos to torus. These transitions are well reported in the literature [49–52] and known as transition from a stable cycle to chaos through a torus break down [48]. The generic character of these transitions has subsequently been confirmed both numerically and experimentally for a wide class of flow [49,50] and discrete time [51,52] systems. Numerical phase portraits and their corresponding power spectra are presented in Fig. 8 and thereby, confirming the corresponding transitions. Each attractor (see Fig. 8) reported here is symmetric with respect to the origin; consequently, they are invariant during the integration under the transformation $(x_1(0), x_2(0), x_3(0), x_4(0))$

Table 2 Summary of the related coexisting attractors in each region of Fig. 7

Region	Route I (magenta color)	Route II (red and blue colors)
A	Symmetric period-1 (Fig. 8e)	Asymmetric pair of periodic attractors [Fig. 3a(1)]
B	Symmetric period-1 (Fig. 8e)	Asymmetric pair of 2D torus [Fig. 3a(2)]
C	Symmetric period-1 (Fig. 8e)	Asymmetric pair of multiperiodic attractors [Fig. 3a(3)]
E	Symmetric period1	Asymmetric pair of periodic and chaotic attractors
F	Symmetric torus attractor (Fig. 8c)	Asymmetric pair of chaotic attractors [Fig. 3a(4)]
G	Symmetric chaotic attractor (Fig. 8a)	Asymmetric pair of chaotic attractors [Fig. 3a(4)]

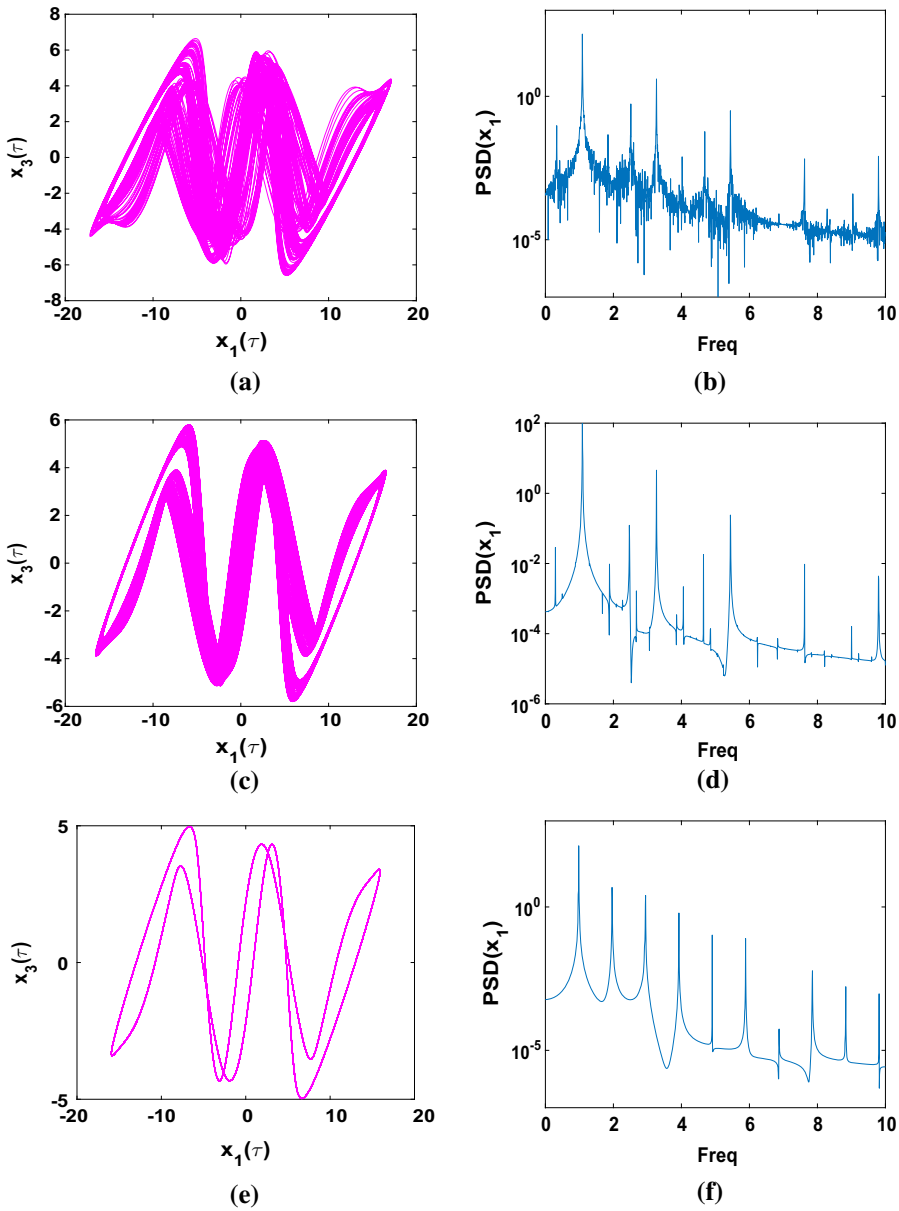

Fig. 8 Numerical phase portraits (left) of the mTCMNL oscillator and their corresponding power spectrum (right) when decreasing α (route I): **a**, **b** Chaotic attractor for $\alpha = 1.0$; **c**, **d** Torus for $\alpha = 0.94$; **e**, **f** Limit cycle for $\alpha = 0.82$; Symmetric attractors (of route **I**) are obtained using the following set of initial conditions (IC) chosen within the basin of attraction of Fig. 9 : $(x_1(0), x_2(0), x_3(0), x_4(0)) = (8.75, -8.75, -5.3, -10.1)$

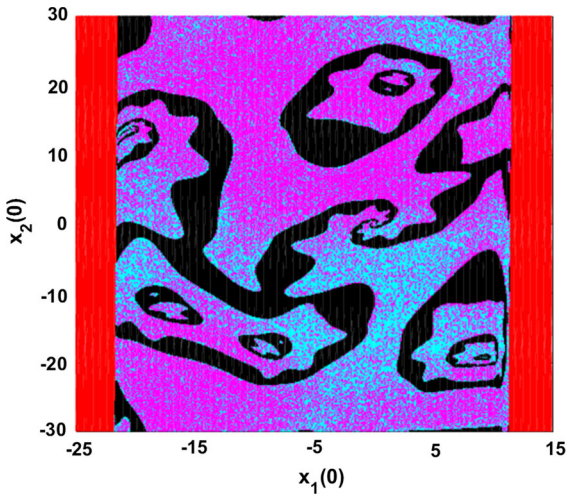

Fig. 9 Basin of initial conditions in the plan $(x_1(0) - x_2(0))$ showing the coexistence of asymmetric pair of chaotic solutions (cyan and magenta) with symmetric quasiperiodic (black) oscillations when the control parameter $\alpha = 0.95$ (region F of Fig. 7); Red areas correspond to unbounded dynamics (color figure online). The other initial conditions are $(x_3(0), x_4(0)) = (-5.3, -10.1)$ and the rest of parameters set are those of Fig. 2

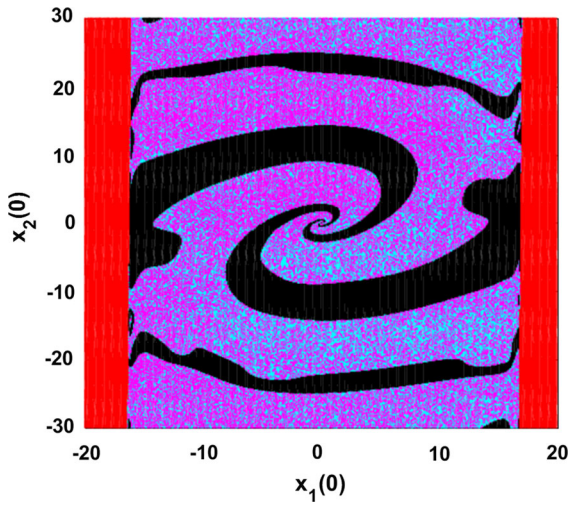

Fig. 10 Cross section of the basin of attraction in the plan $(x_1(0) - x_2(0))$ showing the coexisting region of asymmetric pair of chaotic solutions (cyan and magenta areas) with symmetric limit cycle (black zones) oscillations when the control parameter $\alpha = 0.932$ (region **E** of Fig. 7). Red color corresponds to unbounded dynamics (color figure online) and the other initial conditions are $(x_3(0), x_4(0)) = (0.3, 0.1)$

$\Longleftrightarrow (-x_1(0), -x_2(0), -x_3(0), -x_4(0))$. The scan of initial conditions $(-25 \leq x_1(0) \leq 15$ and $-30 \leq x_2(0) \leq 30)$ in the region F (i.e., for $\alpha = 0.95$) is depicted in Fig. 9. From Fig. 9, the black areas correspond to the domain of initial conditions which lead to quasiperiodic solutions of route **I** (see Fig. 8c), while magenta and cyan zones (in Fig. 9) are domain of initial conditions associated to asymmetric pair of chaotic attractors of route **II** [see Fig. 3a(4)] for fixed parameter sets. Statistical properties of various competing attractors such as maximum Lyapunov exponent and size of attractors were exploited during the computation of basin of attraction. The following set of initial conditions $(8.75, -5.3, -8.75, -10.1)$ has been used to compute quasiperiodic attractor of Fig. 8c, while when choosing $(\pm 0.5, \pm 1.0, \pm 0.5, \pm 0.3)$, we obtained Fig. 3a(4) for fixed parameter sets (i.e., $\alpha = 0.95$). The maximal LE for the fixed control parameter $\alpha = 0.95$ when the system exhibits torus (route **I**) mode is $\lambda_{\max} = -0.0245$ and $\lambda_{\max} = 0.0478$ (route **II**) for chaotic oscillations.

4.2 Route II: from limit cycle oscillation to chaos via 2D-torus

Different scenarios depicted in Fig. 3a(1)–a(4) are presenting the asymmetric pair of attractors when increasing the control parameter α from 0.8 to 0.95 with the following initial conditions: $(x_1(0), x_2(0), x_3(0), x_4(0)) = (\pm 0.5, \pm 1.0, \pm 0.5, \pm 0.3)$. The system undergoes transitions from limit cycle to chaos via destruction of two-dimensional invariant torus. Indeed, for smooth dynamical systems, the basic theorem for the destruction of a two-dimensional torus was proved and the possible ways for the appearance of chaotic dynamics were described in the important work of Afraimovich and Shilnikov [48]. As illustrated in Fig. 7 (see the blue branch of the bifurcation diagram denoted as route **II**), the invariant torus is destroyed in accordance with the classic Afraimovich–Shilnikov scenario [48] through a period doubling bifurcation (see the periodic window **C** in Fig. 7 belonging to the Arnold tongue): as the limit cycle on the 2D torus lost its stability and a period doubling of the resonance cycle took place. Also, many periodic windows are observed during the transition. The basin of initial condition of Fig. 10 (i.e., region **E** of Fig. 7) presents the corresponding state space of initial conditions magnetized by each attractor for fix control parameter $\alpha = 0.932$. One can notice the perfect symmetry of initial conditions in the plane $(x_1(0) - x_2(0))$. Statistical properties of various competing attractors such as maximum Lyapunov exponent and size of attractors were exploited during the computation of basin of attrac-

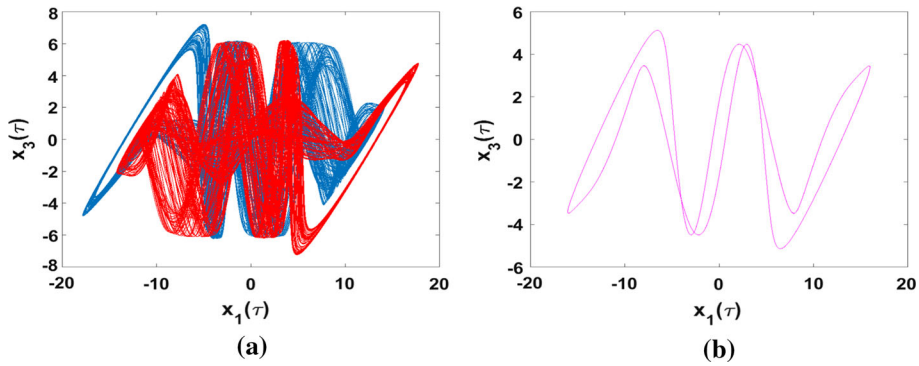

Fig. 11 Numerical phase portraits of asymmetric pair (route II) of chaotic attractors **a** coexisting with period-1 (route I) attractor **b** for $\alpha = 0.932$; Initial conditions to obtain **(a)** are $(x_1(0), x_2(0), x_3(0), x_4(0)) = (\pm 0.5, \pm 1.0, \pm 0.3, \pm 0.1)$ and **(b)** are: $(x_1(0), x_2(0), x_3(0), x_4(0)) = (8.75, -8.75, 0.3, 0.1)$

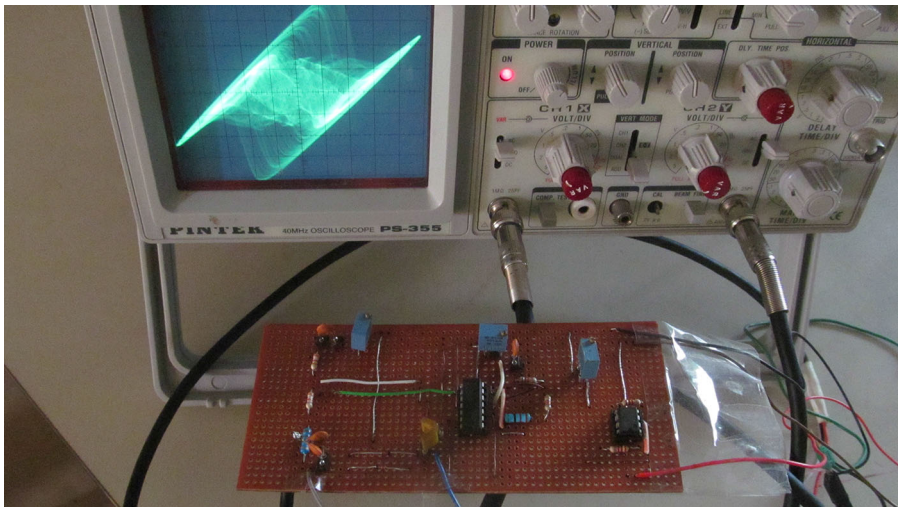

Fig. 12 The experimental mTCMNL circuit in operation. The oscilloscope displays the double-band chaotic attractor captured from the experimental circuit mounted on a breadboard. Discrete components are chosen as : $C_1 = 18.4nF$, $C_2 = 5.7nF$, $L_1 = 15mH$, $L_2 = 1mH$, D1 and D2 are of types 1N4148; $Z_{\text{NIC}} = -R$ is a potentiometer and will serves as control parameter

tion. Henceforth, magenta and cyan colors are associated to asymmetric pair of chaotic attractors (route **II**), while black areas represent the initial conditions for symmetric limit cycle oscillations (route **I**). Red zones correspond to unbounded dynamics (Fig. 10). Initial conditions $x_1(0)$ and $x_2(0)$ are varied in the intervals $[-20, 20]$ and $[-30, 30]$, respectively. Figure 11 presents the obtained (numerically) three coexisting attractors for $\alpha = 0.932$ when varying the initial conditions as in Fig. 10.

5 Experimental results

The implementation of the real-time experimental circuit is a convenient tool to scan the parameter range in order to find the proper parameter values for a numerical simulation [53–55]. Another advantage of such an approach compared to numerical computation is that there is no need to wait for long transient times. Hence, the goal of this section is to implement the real-time experimental circuit of the mTCMNL in order to support and validate numerical results. The schematic diagram of the complete electronic circuit used to investigate the complex dynamical behavior of mTCMNL is shown in Fig. 12. The inductances L_1 and L_2 are simulated here using gyrators [16,23]. It is worth mentioning that the use of gyrators instead of real inductors is advantageous since it becomes possible to monitor the values of inductances/capacitors over a wide range by simply adjusting a resistor. Even though with gyrators the real frequency of the system will be less compared

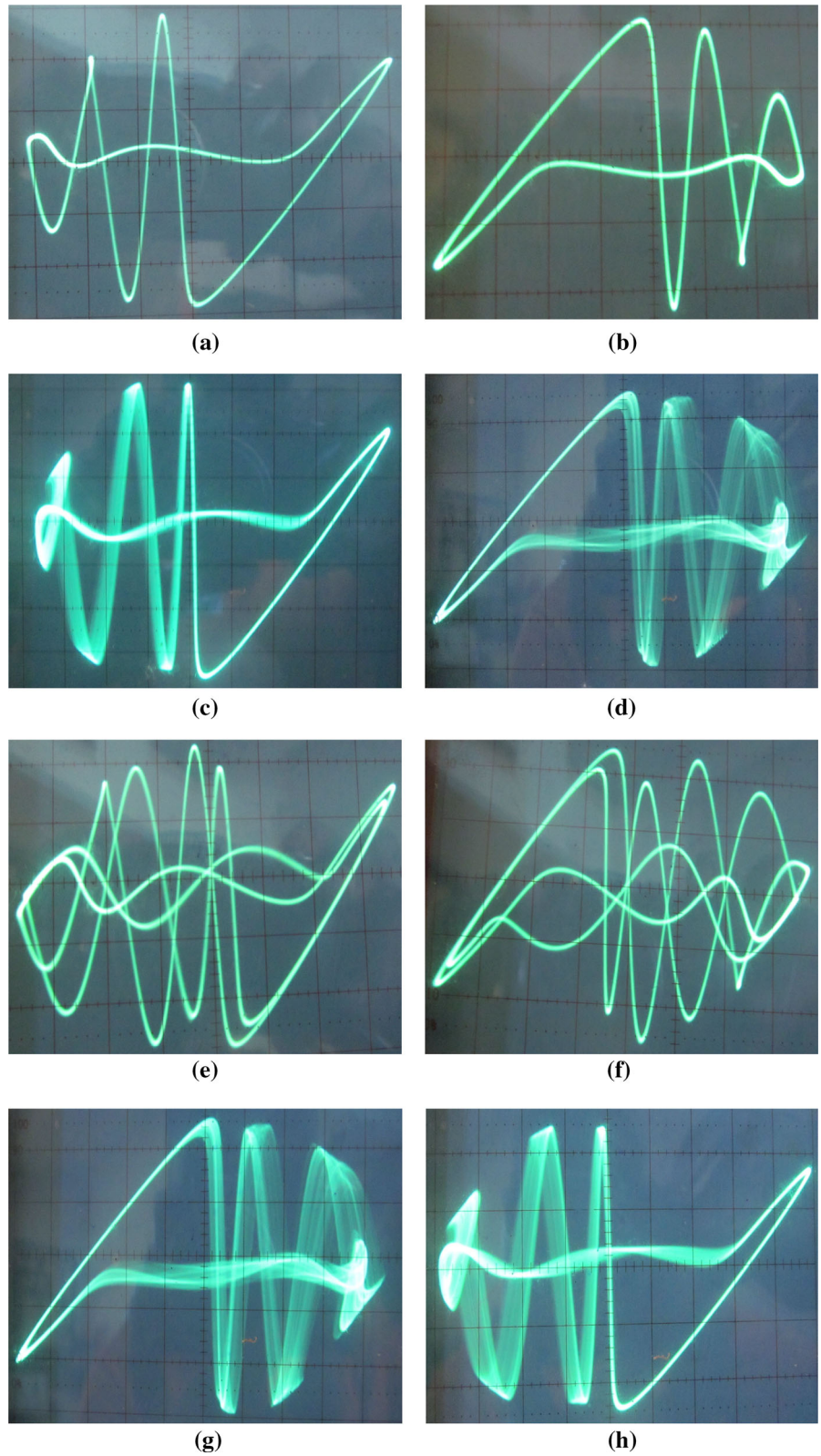

Fig. 13 Experimental phase portraits of the mTCMNL (route II) for real-time circuit implementation obtained using a dual trace oscilloscope in the XY mode. **a**, **b** asymmetric pair of Period-1 attractors for $R = 1090\,\Omega$; **c**, **d** asymmetric pair of quasiperiodic attractor for $R = 1035\,\Omega$; **e**, **f** asymmetric pair of period-2 attractors for $R = 970\,\Omega$; **g**, **h** asymmetric pair of single-band chaotic attractors for $R = 930\,\Omega$; **i**, **j** asymmetric pair of single-band chaotic attractors $R = 880\,\Omega$; **k** symmetric double-band hyperchaos for $R = 866\,\Omega$; **l** symmetric double-band chaos for $R = 800\,\Omega$

Fig. 13 continued

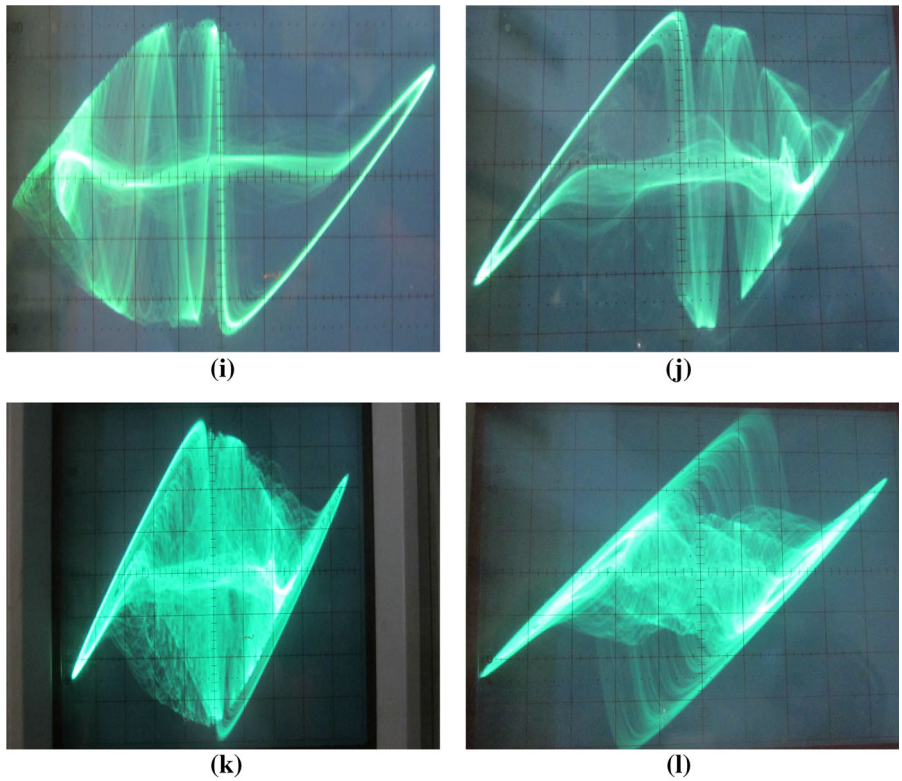

to real inductors because of the narrow band frequency of op. amplifiers, the overall qualitative dynamic of the system will remain the same. The negative impedance converter and the gyrators are built using TL084 and TL082 op. amplifiers with symmetric ± 12 V dc voltage supply. The values of the discrete electronic components used for experiment are provided in Fig. 12.

The experimental results are obtained by slowly monitoring the potentiometer of the negative impedance converter ($Z_{\mathrm{NIC}} = -R$, i.e., varying parameter α) and plotting phase-space trajectories $\left(V_{C_1}, V_{C_2}\right)$ (i.e., (x_1, x_3)) using a PINTEK dual trace oscilloscope in the XY mode. When slowly changing the control resistor R, we found that the experimental mTCMNL circuit exhibits various types of bifurcations. For $R = 1090\,\Omega$, a period-1 limit cycle is observed. When R is gradually decreased, the complete sequence of bifurcation reported previously is observed. The system evolves progressively from period-1 $\rightarrow$ torus state $\rightarrow$ period-2 $\rightarrow$ single-band asymmetric chaotic attractor $\rightarrow$ double-band symmetric hyperchaotic attractor $\rightarrow$ double-band symmetric chaotic attractor. Some windows of periodic behaviors sandwiched within the chaotic domains are also noted. This is clearly illustrated by the experimental pictures of Fig. 13 showing the real time trace of the mTCMNL circuit under consideration. In the light of the pictures in Fig. 13, it can be seen that the real circuit demonstrates the same bifurcation sequences of Fig. 3 as observed during the numerical study (only the capture of route II, i.e., decreasing R (increasing α)). One can notice in Fig. 13 the coexistence of asymmetric pair of attractors for discrete set of control parameters. Such a phenomenon was observed by switching off and on the power supply and thereby randomly selecting initials states.

The coexisting attractor of route I with route II was observed this time by increasing the control parameter R (i.e., decreasing α). During experiments, it was sometimes necessary to heat the discrete components with a hair dryer to randomly select the appropriate initials conditions and thereby obtain the phase portraits of route I as depicted in Fig. 14. The mTCMNL circuit undergoes from symmetric chaotic attractor (Fig. 14a) to limit cycle (Fig. 14c) through torus oscillation (Fig. 14b).

When the control parameter is fixed at $R = 1090\,\Omega$, we observe the coexistence of asymmetric pair of period-1 attractor of Fig. 13a, b with period-1 of

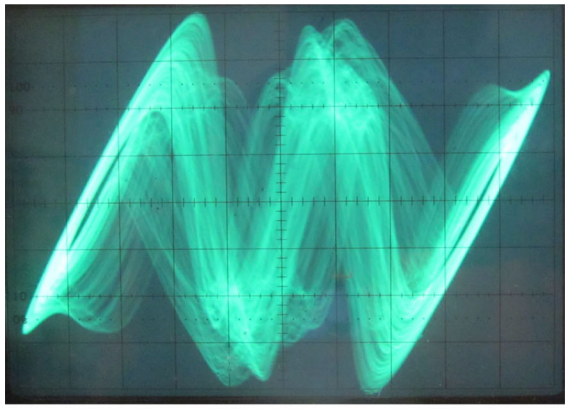

(a)

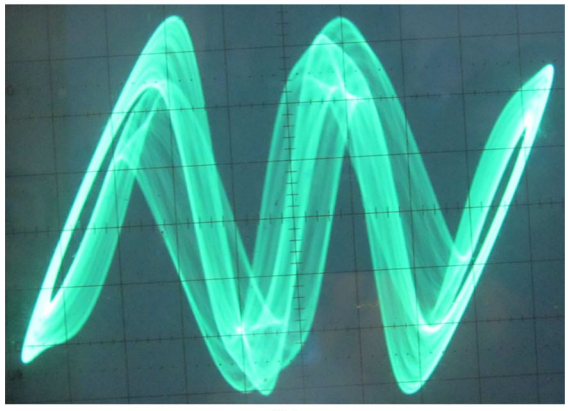

(b)

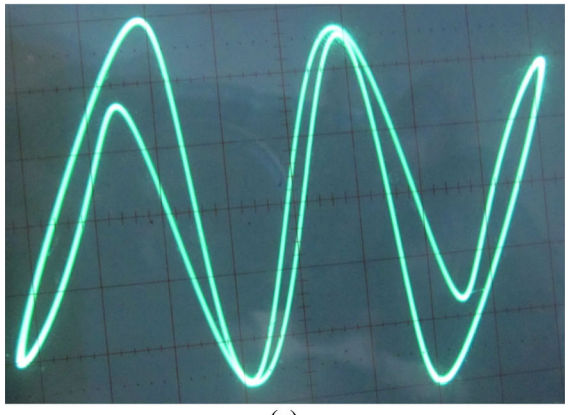

(c)

Fig. 14 Experimental phase portraits of the mTCMNL (route I) when increasing the resistance R traced on a dual PINTEK oscilloscope in XY mode. **a** Chaotic attractor for $R = 880\,\Omega$; **b** Torus for $R = 930\,\Omega$; **c** Period-1 for $R = 1090\,\Omega$

Fig. 14c. Torus of Fig. 14b also coexists with the asymmetric pair of single-band chaotic attractor of Fig. 13g, h for $R = 930\,\Omega$, while chaotic attractor of Fig. 14a coexists with the symmetric pair of chaotic attractor of Fig. 13i, j for $R = 880\,\Omega$. It should be mentioned that chaotic attractors of Fig. 13, with relatively larger basin, are more likely to appear (i.e., more frequent) than those of Fig. 14. Moreover, as expected (owing to the fractal structure of basin boundaries), jumps between coexisting attractors are also observed in experiment. Good agreement can be captured between numerical and experimental results. However, a slight discrepancy that may be attributed to precision on the values of electronic components as well as the simplifying assumptions considered during the modeling process can be noted between numerical and experimental results.

6 Conclusion

This paper has considered the dynamics of the modified TCMNL oscillator by replacing the single diode of the original circuit with two antiparallel ones. The modification yields are relatively simple and provide a nonlinearity capable of rich and interesting phenomena such as torus, hyperchaos and coexistence of multiple attractors. Using standard nonlinear analysis techniques such as bifurcation diagrams, Lyapunov exponent spectrum, Poincaré sections and frequency spectra, the dynamics of the mTCMNL has been characterized in terms of its parameters. Two parameter Lyapunov exponent diagrams have been introduced to characterize chaos, hyperchaos and periodic oscillations as well as their transitions. As a major result, it is found that the mTCMNL exhibits the unusual and striking phenomenon of multiple attractors (i.e., coexistence of asymmetric pair of attractors with a symmetric one) for a wide range of circuits parameters. By changing the initial conditions, asymmetric pair of attractors are coexisting with symmetric one for fix control parameter. Basin of initial conditions of coexisting attractors has been depicted in two different regions. Both hyperchaos and multistability phenomena reported in this work may serve as additional keys for applications such as secure communication (i.e., chaos masking). Results of theoretical analysis are perfectly following laboratory experiments. This clearly shows that the smooth mathematical model based on sine hyperbolic *(I–V)* characteristic of the antiparallel diodes is appropriate to capture detailed behaviors of the such semiconductor diode-based circuits in general. A detail analysis of control and synchronization of each attractor in the

coexisting regions of parameter sets may be carried out in future works. Also, the study performed in this work may easily be extended to similar chaotic and hyperchaotic generators.

Acknowledgements T. F. Fonzin acknowledges firstly DST-FICCI through the C V Raman International Fellowship for African Researchers (INT /NAI/CVRF/2014) for the financial support. Secondly, he acknowledges Mr. Danda Samuel and Mr. Jiogo Guy from National Advanced School of Post and Telecommunication (SUP'PTIC) of Yaoundé-Cameroon for the material grant necessary for experimental analysis. Also, he acknowledges Prof. M. Lakshmanan, Dr. A. Venkatesan and Dr. K. Suresh from Centre for Nonlinear Dynamics (CNLD), Tiruchirappalli, India, for all the helpful discussions and readings. Finally, authors would like to convey thanks to the anonymous reviewers for their useful suggestions and comments that helped to improve the content of the present manuscript.

References

1. Tamasevicius, A., Cenys, A., Mykolaitis, G., Namajunas, A., Lindberg, E.: Hyperchaotic oscillator with gyrators. Electron. Lett. **33**, 542–544 (1997)
2. Pecora, L.M., Carroll, T.L.: Synchronization in chaotic systems. Phys. Rev. Lett. **64**(8), 821 (1990)
3. Louodop, P., Fotsin, H., Kountchou, M., Ngouonkadi, E.B.M., Cerdeira, H.A., Bowong, S.: Finite-time synchronization of tunnel-diode-based chaotic oscillators. Phys. Rev. E **89**(3), 032,921 (2014)
4. Ngouonkadi, E.B.M., Fotsin, H.B., Nono, M.K., Fotso, P.H.L.: Noise effects on robust synchronization of a small pacemaker neuronal ensemble via nonlinear controller: electronic circuit design. Cognit. Neurodyn. **10** (5), 385–404 (2016)
5. Ngouonkadi, E.M., Fotsin, H., Fotso, P.L.: Implementing a memristive van der pol oscillator coupled to a linear oscillator: synchronization and application to secure communication. Phys. Scr. **89**(3), 035,201 (2014)
6. Feki, M.: An adaptive chaos synchronization scheme applied to secure communication. Chaos Solitons Fractals **18**(1), 141–148 (2003)
7. Murali, K., Lakshmanan, M.: Secure communication using a compound signal from generalized synchronizable chaotic systems. Phys. Lett. A **241**(6), 303–310 (1998)
8. Duan, C., Yang, S.: Synchronizing hyperchaos with a scalar signal by parameter controlling. Phys. Lett. A **229**(3), 151–155 (1997)
9. Pérez, G., Cerdeira, H.A.: Extracting messages masked by chaos. Phys. Rev. Lett. **74**(11), 1970 (1995)
10. Matsumoto, T., Chua, L., Kobayashi, K.: Hyper chaos: laboratory experiment and numerical confirmation. IEEE Trans. Circuits Syst. **33**(11), 1143–1147 (1986)
11. Lakshmanan, M., Senthilkumar, D.V.: Dynamics of Nonlinear Time-Delay Systems. Springer, Berlin (2011)
12. Tamaševičius, A., Čenys, A.: Hyperchaos in dynamical systems with a monoactive degree of freedom. Chaos Solitons Fractals **9**(1), 115–119 (1998)
13. Thamilmaran, K., Lakshmanan, M., Venkatesan, A.: Hyperchaos in a modified canonical chua's circuit. Int. J. Bifurc. Chaos **14**(01), 221–243 (2004)
14. Nishio, Y., Mori, S., Saito, T.: Extremely simple hyperchaos generators including one diode. In: 1992 IEEE International Symposium on Circuits and Systems. ISCAS'92. Proceedings, vol. 6, pp. 2797–2800. IEEE (1992)
15. Kengne, J., Chedjou, J., Fozin, T.F., Kyamakya, K., Kenne, G.: On the analysis of semiconductor diode-based chaotic and hyperchaotic generators-a case study. Nonlinear Dyn. **77**(1–2), 373–386 (2014)
16. Fonzin Fozin, T., Kengne, J., Pelap, F.B.: Theoretical analysis and adaptive synchronization of a 4D hyperchaotic oscillator. J. Chaos **2014**, 1–5 (2014)
17. Kengne, J.: Coexistence of chaos with hyperchaos, period-3 doubling bifurcation, and transient chaos in the hyperchaotic oscillator with gyrators. Int. J. Bifurc. Chaos **25**(04), 1550,052 (2015)
18. Jeevarekha, A., Sabarathinam, S., Thamilmaran, K., Philominathan, P.: Analysis of 4D autonomous system with volume-expanding phase space. Nonlinear Dyn. **84**(4), 2273–2284 (2016)
19. Kengne, J., Tabekoueng, Z.N., Fotsin, H.: Coexistence of multiple attractors and crisis route to chaos in autonomous third order Duffing–Holmes type chaotic oscillators. Commun. Nonlinear Sci. Numer. Simul. **36**, 29–44 (2016)
20. Hellen, E.H., Lanctot, M.J.: Nonlinear damping of the LC circuit using antiparallel diodes. Am. J. Phys. **75**(4), 326–330 (2007)
21. Mohammadi, A., Shayegh, F., Abdipour, A., Mirzavand, R.: Direct conversion EHM transceivers design for millimeter-wave wireless applications. EURASIP J. Wirel. Commun. Netw. **2007**(1), 1–9 (2007)
22. Mohyuddin, W., Kim, K.W., Choi, H.C.: Compact wide-band antiparallel diode frequency triplers utilizing planar transitions. Int. J. Antennas Propag. **2015**, 1–7 (2015)
23. Itoh, M.: Synthesis of electronic circuits for simulating nonlinear dynamics. Int. J. Bifurc. Chaos **11**(03), 605–653 (2001)
24. Kengne, J., Njitacke, Z., Nguomkam Negou, A., Fouodji Tsostop, M., Fotsin, H.: Coexistence of multiple attractors and crisis route to chaos in a novel chaotic jerk circuit. Int. J. Bifurc. Chaos **26**(05), 1650,081 (2016)
25. Bao, B., Jiang, T., Xu, Q., Chen, M., Wu, H., Hu, Y.: Coexisting infinitely many attractors in active band-pass filter-based memristive circuit. Nonlinear Dyn. **86**(3), 1711–1723 (2016)
26. Bao, B., Li, Q., Wang, N., Xu, Q.: Multistability in chua's circuit with two stable node-foci. Chaos Interdiscip. J. Nonlinear Sci. **26**(4), 043,111 (2016)
27. Sprott, J.C., Wang, X., Chen, G.: Coexistence of point, periodic and strange attractors. Int. J. Bifurc. Chaos **23**(05), 1350,093 (2013)
28. Ngouonkadi, E.M., Fotsin, H., Fotso, P.L., Tamba, V.K., Cerdeira, H.A.: Bifurcations and multistability in the extended Hindmarsh–Rose neuronal oscillator. Chaos Solitons Fractals **85**, 151–163 (2016)
29. Sprott, J.C., Li, C.: Asymmetric bistability in the Rössler system. Acta Phys. Pol. B **48**(1), 97 (2017)
30. Jafari, S., Sprott, J.: Simple chaotic flows with a line equilibrium. Chaos Solitons Fractals **57**, 79–84 (2013)

31. Cushing, J.M., Henson, S.M., Blackburn, C.C.: Multiple mixed-type attractors in a competition model. J. Biol. Dyn. **1**(4), 347–362 (2007)
32. Upadhyay, R.K.: Multiple attractors and crisis route to chaos in a model food-chain. Chaos Solitons Fractals **16**(5), 737–747 (2003)
33. Rinaldi, S., Muratori, S., Kuznetsov, Y.: Multiple attractors, catastrophes and chaos in seasonally perturbed predator-prey communities. Bull. Math. Biol. **55**(1), 15–35 (1993)
34. Masoller, C.: Coexistence of attractors in a laser diode with optical feedback from a large external cavity. Phys. Rev. A **50**(3), 2569 (1994)
35. Pisarchik, A.N., Feudel, U.: Control of multistability. Phys. Rep. **540**(4), 167–218 (2014)
36. Kengne, J., Negou, A.N., Tchiotsop, D.: Antimonotonicity, chaos and multiple attractors in a novel autonomous memristor-based jerk circuit. Nonlinear Dyn. **88**(4), 2589–2608 (2017)
37. Alombah, N.H., Fotsin, H., Romanic, K.: Coexistence of multiple attractors, metastable chaos and bursting oscillations in a multiscroll memristive chaotic circuit. Int. J. Bifurc. Chaos **27**(05), 1750,067 (2017)
38. Sprott, J.C.: Elegant Chaos: Algebraically Simple Chaotic Flows. World Scientific, Singapore (2010)
39. Morfu, S., Nofiele, B., Marquié, P.: On the use of multistability for image processing. Phys. Lett. A **367**(3), 192–198 (2007)
40. Sharma, P., Shrimali, M., Prasad, A., Kuznetsov, N., Leonov, G.: Control of multistability in hidden attractors. Eur. Phys. J. Spec. Top. **224**(8), 1485–1491 (2015)
41. Aronson, D., Chory, M., Hall, G., McGehee, R.: Bifurcations from an invariant circle for two-parameter families of maps of the plane: a computer-assisted study. Commun. Math. Phys. **83**(3), 303–354 (1982)
42. Wolf, A., Swift, J.B., Swinney, H.L., Vastano, J.A.: Determining Lyapunov exponents from a time series. Physica D **16**(3), 285–317 (1985)
43. Stegemann, C., Albuquerque, H.A., Rubinger, R.M., Rech, P.C.: Lyapunov exponent diagrams of a 4-dimensional chua system. Chaos Interdiscip. J. Nonlinear Sci. **21**(3), 033,105 (2011)
44. Rech, P.C.: Hyperchaos and quasiperiodicity from a fourdimensional system based on the Lorenz system. Eur. Phys. J. B **90**(12), 251 (2017)
45. Marwan, N., Wessel, N., Meyerfeldt, U., Schirdewan, A., Kurths, J.: Recurrence-plot-based measures of complexity and their application to heart-rate-variability data. Phys. Rev. E **66**(2), 026,702 (2002)
46. Thiel, M., Romano, M.C., Kurths, J.: How much information is contained in a recurrence plot? Phys. Lett. A **330**(5), 343–349 (2004)
47. Franceschini, V.: Bifurcations of tori and phase locking in a dissipative system of differential equations. Physica D **6**(3), 285–304 (1983)
48. Afraimovich, V., Shilnikov, L.P.: Invariant two-dimensional tori, their breakdown and stochasticity. Am. Math. Soc. Transl. **149**(2), 201–212 (1991)
49. El Aroudi, A., Benadero, L., Toribio, E., Machiche, S.: Quasiperiodicity and chaos in the dcdc buckboost converter. Int. J. Bifurc. Chaos **10**(02), 359–371 (2000)
50. Letellier, C., Messager, V., Gilmore, R.: From quasiperiodicity to toroidal chaos: analogy between the Curry–Yorke map and the van der pol system. Phys. Rev. E **77**(4), 046,203 (2008)
51. Maistrenko, Y.L., Popovych, O.V., Tass, P.A.: Chaotic attractor in the Kuramoto model. Int. J. Bifurc. Chaos **15**(11), 3457–3466 (2005)
52. Zhusubaliyev, Z.T., Mosekilde, E.: Novel routes to chaos through torus breakdown in non-invertible maps. Physica D **238**(5), 589–602 (2009)
53. Maurer, J., Libchaber, A.: Rayleigh–Bénard experiment in liquid helium; frequency locking and the onset of turbulence. Journal de Physique Lettres **40**(16), 419–423 (1979)
54. Alombah, N.H., Fotsin, H., Ngouonkadi, E.M., Nguazon, T.: Dynamics, analysis and implementation of a multiscroll memristor-based chaotic circuit. Int. J. Bifurc. Chaos **26**(08), 1650,128 (2016)
55. Kountchou, M., Louodop, P., Bowong, S., Fotsin, H., et al.: Analog circuit design and optimal synchronization of a modified Rayleigh system. Nonlinear Dyn. **85**(1), 399–414 (2016)